PCCP

RSC Publishing

PAPER

View Article Online
View Journal | View Issue

Structural prediction of a rhodamine-based biosensor and comparison with biophysical data†

Cite this: *Phys. Chem. Chem. Phys.*, 2013, **15**, 2177

Marcos Brown Gonçalves,‡[ab] Jens Dreyer,‡[ab] Paola Lupieri,[ab] Claudia Barrera-Patiño,[ab] Emiliano Ippoliti,[ab] Martin R. Webb,[c] John E. T. Corrie[c] and Paolo Carloni*[ab]

Received 14th July 2012,
Accepted 30th November 2012

DOI: 10.1039/c2cp42396k

www.rsc.org/pccp

The predicted structure has been calculated for a protein-based biosensor for inorganic phosphate (Pi), previously developed by some of us (Okoh *et al.*, *Biochemistry*, 2006, **45**, 14764). This is the phosphate binding protein from *Escherichia coli* labelled with two rhodamine fluorophores. Classical molecular dynamics and hybrid Car–Parrinello/molecular mechanics simulations allow us to provide molecular models of the biosensor both in the presence and in the absence of Pi. In the latter case, the rhodamine fluorophores maintain a stacked conformation in a 'face A to face B' orientation, which is different from the 'face A to face A' stacked orientation of free fluorophores in aqueous solution (Ilich *et al.*, *Spectrochim. Acta*, *Part A*, 1996, **52**, 1323). A protein conformation change upon binding Pi prevents significant stacking of the two rhodamines. In both states, the rhodamine fluorophores form hydrophobic contact with LEU291, without establishing significant hydrogen bonds with the protein. The accuracy of the models is established by a comparison between calculated and experimental absorption and circular dichroism spectra.

Published on 17 December 2012 on http://pubs.rsc.org | doi:10.1039/C2CP42396K
Downloaded by Library for Natural Sciences of the RAS on 15/05/2013 11:41:24.

1 Introduction

Fluorescence probes are routinely used to investigate the structural basis of biochemical processes *in vitro* and *in vivo*, yet details of the structural interactions that affect their optical properties are still poorly understood. A typical system is the rhodamine-based fluorescent biosensor suitable for real-time measurements of inorganic phosphate (Pi), a product of many enzymatic reactions and an important assay target for the study of cellular activities.[1] The sensor uses the phosphate binding protein (PBP) from *Escherichia coli* as a scaffold.[1] PBP binds Pi very specifically and tightly with a well-defined conformation change.[2–4] This structural change has been exploited in the development of the sensor.[1,5] Two tetramethylrhodamines (RHO, Fig. 1, upper panel) were covalently attached to mutation-generated cysteines (A17C, A197C) on the surface of the protein, using 6-iodoacetamidotetramethylrhodamine (Fig. 1, lower panel).[6] A17 and A197 were selected to obtain a large change in the relative positions of the two fluorophores upon the conformation change due to Pi binding.[1] In the resulting adduct, RHO_2–PBP·Pi, the fluorescence emission of the rhodamines increases 18-fold when Pi binds to the sensor.[1,7] These changes suggested that Pi binding causes disruption of a stacked dimeric conformation of the RHOs (Fig. 1, lower panel), which is known to quench their emission.[8–11]

Similar features have been observed for a rhodamine dimer in water.[8,9,12,13] This property has also been used previously in a number of assays, *e.g.* on peptides separated by protease cleavage,[14,15] oligonucleotides,[16,17] or ribosomal proteins.[18] The enhanced fluorescence upon Pi binding to the sensor protein is accompanied by a change in the visible absorption spectrum of the rhodamines.[1] However, unlike the situation in the examples quoted above,[14–18] where a change in the biochemical state results in complete dissociation of the two rhodamines and reversal of the absorption to that of a monomeric rhodamine, in the present case the visible absorption spectrum shows only a partial change and remains much perturbed from the monomer spectrum. Thus, the two rhodamines are likely to retain a certain degree of electronic interaction even in the Pi-bound form of the complex

[a] *Computational Biophysics, German Research School for Simulation Sciences,§ D-52425 Jülich, Germany. E-mail: p.carloni@grs-sim.de*
[b] *Institute for Advanced Simulation, Forschungszentrum Jülich, D-52425 Jülich, Germany*
[c] *MRC National Institute for Medical Research, The Ridgeway, Mill Hill, London, NW71AA, UK*

† Electronic supplementary information (ESI) available: Clustering and RMSD analyses; CD spectrum; MD trajectory analyses: Pi coordination data, protein–fluorophore close contacts and fluorophore–fluorophore analyses; and Kohn–Sham molecular orbitals. See DOI: 10.1039/c2cp42396k

‡ Both authors contributed equally.

§ Joint venture of RWTH Aachen University and Forschungszentrum Jülich, Germany.

Downloaded by Library for Natural Sciences of the RAS on 15/05/2013 11:41:24.
Published on 17 December 2012 on http://pubs.rsc.org | doi:10.1039/C2CP42396K

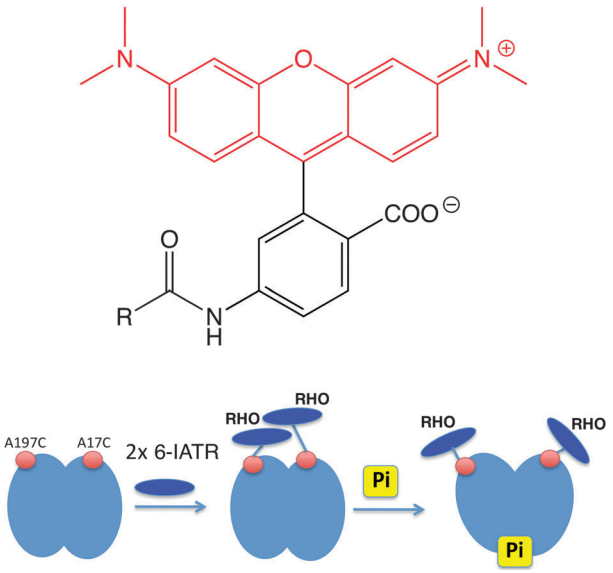

Fig. 1 The upper panel shows the rhodamine fluorophore (RHO), with the xanthylium ring system that is responsible for fluorescence highlighted in red. For the labelling reagent 6-iodoacetamidotetramethylrhodamine (6-IATR), R = CH_2I. When covalently attached to the protein, the sulfur atom of a cysteine residue replaces the iodide group, giving the RHO substituent as shown. The lower panel shows the principle of the sensor in schematic form.

presumably because the two rhodamines remain held in proximity by the protein scaffold.

Experimental difficulties have prevented elucidation of an atomic resolution structure of RHO_2–PBP by X-ray crystallography or NMR spectroscopy, so structural features that underlie the absorbance and fluorescence changes could not be investigated. Here, we use molecular simulations to predict structural determinants of RHO_2–PBP and RHO_2–PBP·Pi.

Classical molecular dynamics (MD) simulations are used to construct the molecular models. Then, a hybrid density functional theory (DFT) approach employing Car–Parrinello[19]/Molecular Mechanics (CP/MM) simulations[20] at room temperature is used. Finally, circular dichroism (CD) and optical spectra are obtained so that comparison with experimental data allows us to validate the models. For the simulation of optical spectra, time-dependent DFT (TDDFT)[21] is employed on snapshots from the CP/MM trajectory. The approach used here takes fully into account environmental effects of the protein and the aqueous solution as well as inhomogeneous spectral broadening due to room temperature fluctuations of the entire system. This approach has been shown to give fairly good results for a variety of solutes in aqueous solution.[22–26]

2 Computational methods

The structures of RHO_2–PBP and RHO_2–PBP·Pi were built based on the X-ray structure of T141D PBP[27] and of PBP in complex with Pi,[2,28] respectively. The structure of apo PBP was obtained manually by replacing D with T. The A17C and A197C mutations were inserted manually on the X-ray structures of PBP in the presence[3] and absence[27] of Pi. Care was taken to avoid clashes with other residues. The two RHO fluorophores were attached to CYS17 and to CYS197 on the surface of the protein in both PBP·Pi and apo PBP. The complexes were inserted into a box with edges of 72.5 × 91 × 73.9 $Å^3$, containing ~14 700 water molecules, in total ~48 700 atoms.

In both the MD and QM/MM calculations, the AMBER parm99 force field[29] was used to describe the protein. The partial charges for the Pi compound, as well as the residues close to it, were calculated by performing a standard RESP parameterization[30] based on gas phase DFT calculations of the respective reduced model (see ESI†). Bond parameters for Pi and its adjacent environment were tuned, in order to reproduce the structural parameters from the reduced model. The TIP3P model was adopted to describe water molecules.[32] In the MD simulations, from the reduced model we built and parameterized the RHO fluorophores following ref. 31 in which the determinants of *N*,*N*,*N*′,*N*′-tetramethylrhodamine in aqueous solution were obtained by DFT analysis.

Periodic boundary conditions were applied. A smooth PME method[33] with 90 wave vectors in each dimension and fourth-order cubic interpolation was used to treat the long-range electrostatic interactions. A cut-off of 12 Å was used for the real part of the electrostatic interactions as well as for the van der Waals interactions. After a preliminary minimization both systems underwent 11–16 ns of MD simulations at room temperature and pressure with the NAMD package[34] and keeping the temperature constant by using ordinary Langevin dynamics. For pressure control a modified Nosé–Hoover method was employed in which Langevin dynamics was applied to control fluctuations in the barostat.[35,36] A time step of 1 fs was applied. Clustering analyses were performed using a cutoff criterion of 0.14 nm RMSD as described by Daura *et al.*[37]

In the hybrid CP/MM MD simulations the positively charged 3,6-bis(dimethylamino)xanthylium cation moiety was considered as the QM part (38 atoms, *cf.* Fig. 1, upper panel, highlighted part in red). Test calculations showed that larger QM parts, taking also the benzoic acid moiety into account, do not significantly affect the absorption spectra. In RHO_2–PBP, both xanthylium cations were included in the QM part (76 atoms). For RHO_2–PBP·Pi the two rhodamines were separated during the classical MD, maintaining the configuration with largely reduced interaction. Therefore, the chromophores were considered independently as the QM part in two different CP/MM MD simulations. The QM part was described at the DFT-BLYP level,[38,39] while the rest was treated at the force field level as in the initial classical MD simulations. An adapted monovalent carbon pseudopotential was employed to saturate the dangling bonds in between the QM and MM regions.[40] The full Hamiltonian approach[20] implemented in the CPMD/Gromos program[41,42] was used to interface the QM and MM regions. The wave functions were expanded in a plane wave basis set up to a cut-off of 70 Ry. The atomic all-electron potentials were described with norm-conserving, London dispersion-corrected Troullier–Martins pseudopotentials[43,44] and the Kleinman–Bylander approach was used to treat their non-local parts.[45] Isolated system conditions within the plane wave formalism were achieved using the scheme of Martyna and Tuckerman.[46] 5 ps-long CP/MM dynamics calculations[20,47] were performed for the 2 most populated clusters from the

 This journal is © the Owner Societies 2013

Published on 17 December 2012 on http://pubs.rsc.org | doi:10.1039/C2CP42396K
Downloaded by Library for Natural Sciences of the RAS on 15/05/2013 11:41:24.

classical MD trajectories. Hydrogen bonds between the RHO fluorophores and PBP were identified using a distance between heavy atoms up to 3.6 Å and an angle cut-off of 30 degrees. For contact analyses the following distance criteria were used to identify close contacts: $d < 4.1$ Å between H atoms and $d < 5.1$ Å between heavy atoms (carbon, nitrogen and oxygen) of both RHO and PBP residues.

Absorption spectra were computed by averaging results from TDDFT[21] calculations on 40 CP/MM snapshots taken from all calculated CP/MM trajectories. Line spectra obtained for single snapshots were convoluted with a Gaussian function with an empirically determined width of 0.03 eV. The convergence issue was tackled considering several snapshots taken at equidistant time intervals from the equilibrated CP/MM trajectory. This analysis suggests that, depending on the system, about 20–40 sets of excitation calculations are sufficient to obtain converged spectra. Experimental visible absorption spectra in aqueous solution have been reported in ref. 1.

CD spectra were recorded using the web interface DichroCalc developed by Hirst *et al.*[48,49] with parameters derived *ab initio*.[50] Chromophores included in the simulation are backbone peptide bonds[50] including charge-transfer between adjacent groups[51] and tryptophan side chain chromophores.[52] Experimental CD spectra are given in ref. 4.

3 Results and discussion

3.1 Structural model for RHO_2–PBP·Pi

The structure of the protein is well maintained during the MD simulations, as shown by a superposition of the initial structure of RHO_2–PBP·Pi taken from X-ray experiments for PBP[2,27,28] and the final structure of the classical MD simulation (Fig. 2a). A plot of the RMSD as a function of simulated time (Fig. S1a, ESI†) suggests that the structures are equilibrated after about 3 ns. The two most populated clusters, which represent about 60% of the trajectory occupation (Fig. S2a, ESI†), were considered for subsequent CP/MM simulations. The recorded CD spectrum (Fig. S3, ESI†), which is based on amide group absorption and is characteristic of the secondary structure, reproduces the broad negative peak at around 210 nm.[4]

In the X-ray structure[28] Pi forms hydrogen bonds (H-bonds) with THR10, THR141, GLY140, SER38, and PHE11 NH groups, with SER139, THR141, and SER38 OH side chains, as well as with the guanidinium group of ARG135 and the side-chain carboxylate of ASP56.[28] The Pi coordination is fairly well preserved during the dynamics, although the Pi H-bonds are longer in the MD structure than in the X-ray structure (Fig. 3; Fig. S4 and Table S1, ESI†). In addition, ASP56 forms 2 H-bonds in the MD structure whilst only one is observed in the initial experimental structure. However, THR10 and PHE11 form 3 H-bonds in the initial model, but not in the MD structures.

The two RHOs in RHO_2–PBP·Pi are positioned in a monomer-like configuration (Fig. 2a and 4a) during the entire MD. They experience large fluctuations as evidenced by the RMSD variations of the fluorophores that are particularly large for RHO17 (see Fig. S1a, ESI†). Likewise, the dihedral angle between the xanthylium

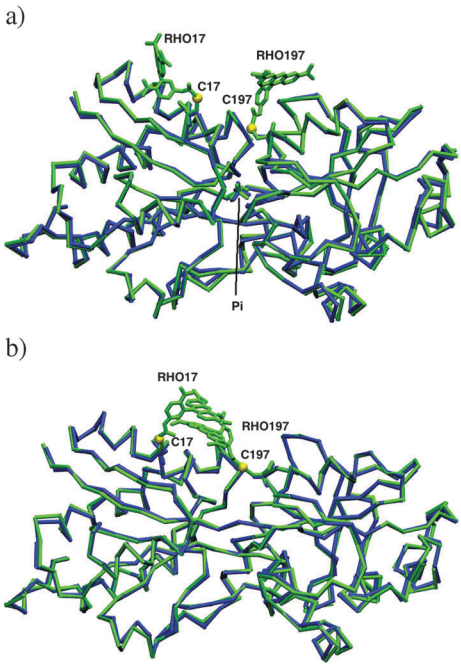

Fig. 2 (a) RHO_2–PBP·Pi: superposition of C_α trace representations of the initial structure (blue), derived from X-ray experiments[2,27,28] and final MD structure (green). The protein is a single chain with two domains consisting of α-helix and β-sheet elements.[2,27] The deep cleft in between tightly binds the analyte Pi. The two RHO fluorophores (residue names RHO197 and RHO17) are largely separated from each other. (b) RHO_2–PBP: superposition of initial (blue) structures, derived from X-ray experiments[27] and final (green) structures of classical MD simulations for RHO_2–PBP. The two RHO fluorophores RHO197 and RHO17 maintain a stable stacked 'face A to face B' dimer configuration. Face A is that side of the xanthylium system adjacent to the carboxylate group on the pendant aryl ring, whereas face B is the side of the xanthylium system that is distal to the carboxylate.

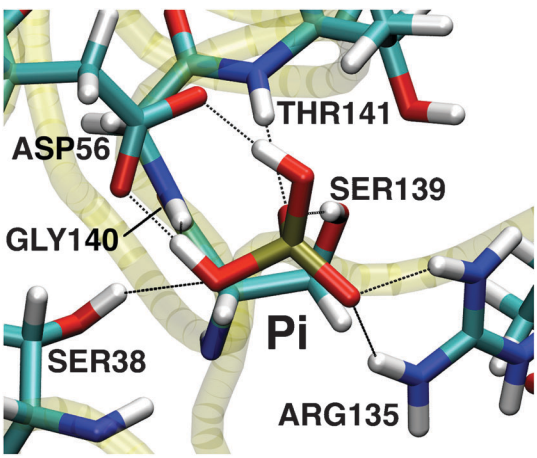

Fig. 3 Representative of the most populated cluster from the classical MD simulation for Pi coordination in RHO_2–PBP·Pi.

and the aryl groups fluctuates between 65° and 130° in RHO17, whereas it remains stable at about 65° in RHO197 (Fig. S9, ESI†). This supports the conclusions from fluorescence experiments,[1] which attribute the large increase of fluorescence upon Pi binding

Published on 17 December 2012 on http://pubs.rsc.org | doi:10.1039/C2CP42396K
Downloaded by Library for Natural Sciences of the RAS on 15/05/2013 11:41:24.

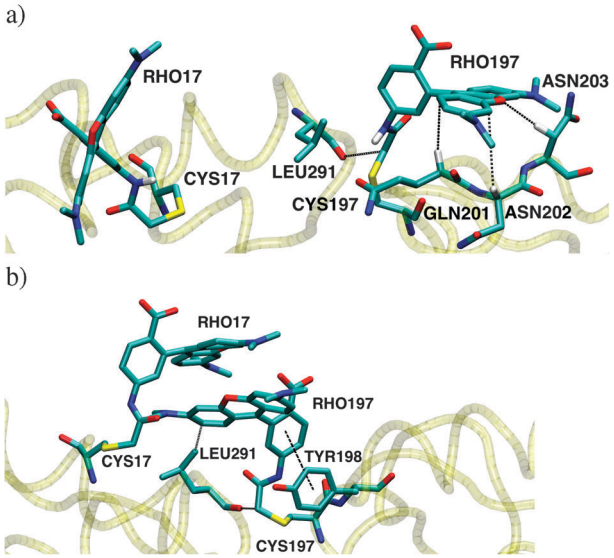

Fig. 4 Representatives of the most populated clusters from the classical MD simulations showing the connection of two rhodamines to the respective cysteine residues as well as interactions between the rhodamines and PBP. (a) RHO_2–PBP·Pi: contacts of RHO197 with LEU291, ASN202, ASN203 and GLN201. RHO17 does not exhibit any persistent interactions with PBP. (b) RHO_2–PBP: contacts of RHO197 with TYR198 and LEU291.

to disruption of the stacked RHO dimer conformation assumed for RHO_2–PBP, thus inhibiting emission quenching.

The two fluorophores do not form stable H-bond interactions. However, RHO197 forms hydrophobic interactions with LEU291, which is in close contact with the tail of the RHO197 benzoate ring (Fig. 4a) over the entire trajectory, as well as with GLN201, ASN202 and ASN203 (Table 1, see also Fig. S5, ESI†). In contrast, RHO17 does not show any persistent interactions with PBP.

The calculated absorption spectrum (Table 2) is shifted to lower wavelength with respect to the experimental one by about 70 nm ($\approx$0.4 eV). We mostly attribute this shift to the BLYP functional within the TDDFT approach, for which similar absolute errors have been found previously.[53,54] It should be noted that the choice of functionals within our computational approach based on plane wave expansions of the wave function is restricted to gradient-corrected functionals of similar quality to BLYP. The spectrum shows a broad band with an implied

Table 1 Selected average contact distances (with standard deviation) in Å in the classical MD simulations of RHO_2–PBP·Pi and RHO_2–PBP

Contact	RHO_2–PBP·Pi	RHO_2–PBP
RHO197:C-LEU291:O	3.69 ± 0.41	3.72 ± 0.42
RHO197:C-LEU291:C	—	4.23 ± 0.48
RHO197:N-ASN202:H	5.10 ± 1.28	—
RHO197:O-ASN203:C	4.05 ± 1.64	—
RHO197:N-GLN201:O	3.17 ± 0.69	—
RHO197:X-TYR198:X[a]	—	4.95 ± 1.06

[a] For RHO197–TYR198 the distance is defined in between the centres of mass of the phenyl rings of the RHO197 benzoate side group and the TYR198 side chain (see Fig. 4b).

Table 2 Experimental and calculated excitation energies

	Experiment[1]		Simulation	
	[nm]	[eV]	[nm]	[eV]
RHO_2–PBP·Pi	556 (w)	2.2		
	517 (s)	2.4	450	2.8
RHO_2–PBP	554 (vw)	2.2	490	2.5
	515 (s)	2.4	435	2.8

shoulder on the red side, but no individual peaks as in the experimental spectrum are resolved (Fig. 5).

An analysis of the electronic spectra of RHO_2–PBP·Pi shows that the broad band arises from contributions of intense and narrow $\pi \rightarrow \pi^*$ HOMO $\rightarrow$ LUMO excitations overlapped with weak, but widely spread, combinations of two transitions. The first was $\pi \rightarrow \pi^*$ HOMO $-$ 1 $\rightarrow$ LUMO and HOMO $\rightarrow$ LUMO centred at the red part of the band and the second was $\pi \rightarrow \pi^*$ HOMO $-$ 1 $\rightarrow$ LUMO, centred at the blue part of the band (*cf.* Fig. S11, ESI†). An energetic separation in terms of two different centres of these contributions, as evident from the experimental spectrum, cannot be deduced from the simulation data. However, the simulated band shape does reflect the experimentally observed intensity redistribution between the two peaks on going from a free rhodamine monomer in water to protein-bound RHOs in a monomer-like conformation as in RHO_2–PBP·Pi. TDDFT studies were combined with a polarizable continuum model (PCM) in a related rhodamine chromophore in water using vertical excitations at a ground state optimized geometry.[55,56] These studies reported a single peak in the relevant spectral region with a similar description of the character of the electronic transition. The method was extended to a multilevel approach combining classical MD simulations with subsequent single-point TDDFT calculations on a selection of MD snapshots.[57] In contrast, this revealed a broad band with two shoulders as observed experimentally though with a different intensity distribution.

3.2 Structural model for RHO_2–PBP

The structure of RHO_2–PBP is similar to the experimental X-ray structure[3] and remains stable along the MD (Fig. 2b). A plot of

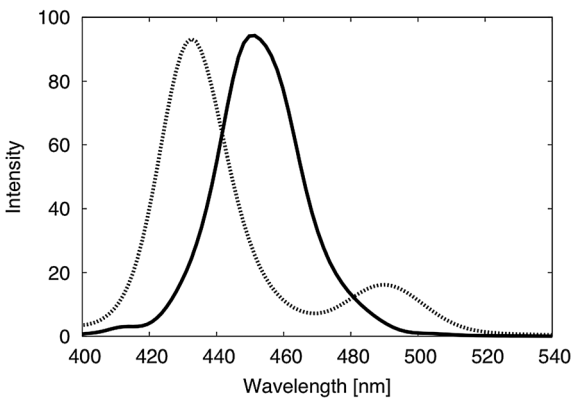

Fig. 5 Simulated absorption spectra of RHO_2–PBP·Pi (solid line) and (b) RHO_2–PBP (dashed line). The intensity scale has arbitrary units.

 This journal is © the Owner Societies 2013

Published on 17 December 2012 on http://pubs.rsc.org | doi:10.1039/C2CP42396K
Downloaded by Library for Natural Sciences of the RAS on 15/05/2013 11:41:24.

the RMSD as a function of simulated time (Fig. S1b, ESI†) reveals that the structures are equilibrated after about 3 ns. Cluster analysis was performed showing two clusters with the sum of occupation around 70% (Fig. S2b, ESI†). The two RHO molecules adopt a novel stacked 'face A to face B' dimer arrangement with the carboxylate groups pointing in the same direction (Fig. 2b and 4b, see also Fig. S10, ESI†). This is in contrast to the usual situation for rhodamine dimers in water or in the crystal phase, which adopt either a 'face B to face B' or a 'face A to face A' configuration.[1,13,31] Face A is that side of the xanthylium system adjacent to the carboxylate group on the pendant aryl ring, whereas face B is the side of the xanthylium system that is distal to the carboxylate. Note that a steric barrier prevents free rotation about the bond that joins the xanthylium system and the pendant aryl ring so that the two faces maintain separate identities (Fig. S10, ESI†). In RHO197, the rhodamine of the dimer makes contact with the protein, the carboxylate group points away from the protein surface towards the solvent. This preference of rhodamines, presumably driven by hydrophobic effects, has been noted previously.[58] The degree of π–π interaction between the two xanthyliums is evaluated by measuring the distance between the geometric centres of the three rings in the xanthylium moieties as well as the angle between the normal vectors of the respective ring planes (Fig. S7–S10, ESI†). In the first 5 ns of the classical MD trajectory distances vary between 4 and 9 Å. Thereafter the inter-ring separation becomes stabilized, with a skewed relationship between the two xanthylium moieties, characterized by a gradual increase in the separation between the individual paired rings of the two groups *i.e.* $r_{aa} = 4.2 \pm 0.8$ Å, $r_{bb} = 4.4 \pm 0.7$ Å and $r_{cc} = 5.0 \pm 0.7$ Å (see Fig. S7 and S10, ESI†). The angle between the normal vectors, which is 0° for ideal π–π stacking with parallel ring planes, fluctuates between 0° and 70° with an average value of 23° ± 11° (Fig. S8, ESI†). This analysis thus reveals a stable and slightly angled stacked conformation of the two xanthylium systems. It is also noted that the dihedral angle between the pendant aryl group and the xanthylium system, normally close to 90°, is distorted, fluctuating between 70° and 130° more frequently for the RHO17 residue (Fig. S9, ESI†). All of these perturbations from a "normal" rhodamine dimer structure must arise from constraints imposed by the tethers to the protein scaffold.

The calculated CD spectrum (Fig. S3, ESI†) is very similar to the one for RHO_2–PBP·Pi indicating that the uptake of Pi does not change the secondary structure content significantly, in accordance with experimental results.[4] The structural analysis of the RHO_2–PBP complex reveals only a single H-bond between the rhodamine and the protein that appears in more than 5% of the trajectory,[59] though primarily in the initial part of the trajectory and therefore not considered relevant.

The fluorophore in contact with the protein (RHO197) forms direct hydrophobic interactions with TYR198 and LEU291 (Fig. 4b and Table 1). The two aromatic rings of RHO197 and TYR198 maintain π–π interactions with an average distance of 4.9 ± 1.0 Å between the centres of mass of the phenyl rings of the RHO197 benzoate side group and the TYR198 side chain (Fig. S6, ESI†). LEU291 always stays close to RHO197 with an average value of 3.7 ± 0.4 and 4.2 ± 0.5 Å for the minimum heavy atom distance, which can be attributed to hydrophobic interactions. The RHO197 fluorophore interacts with TYR198 and LEU291, the latter being the only residue in contact with the RHOs in both RHO_2–PBP and RHO_2–PBP·Pi. This suggests that mutations of these two residues could have considerable influence on the structural properties of the fluorophore–protein complex, which is expected to be reflected in the change of optical properties.

The simulated absorption spectrum of RHO_2–PBP plotted in Fig. 5 is blue shifted by about 60–80 nm from the experimentally observed peak, and a similar shift was observed in the spectrum recorded for RHO_2–PBP·Pi (Table 2). The spectrum shows two peaks with an intensity ratio in agreement with that obtained by experiment[1] and a splitting of about 0.3 eV, which is somewhat larger than that observed experimentally (≈0.2 eV). The shift between the two intense peaks in the RHO_2–PBP·Pi and RHO_2–PBP spectra was ≈20 nm and it is possibly due to the different model adopted, which considers the two xanthylium chromophores separately in different calculations with a charge of +1*e* each *versus* a xanthylium dimer with a total charge of +2*e*.

Analysis of the most intense transitions for RHO_2–PBP among all snapshots reveals that the strong peak at about 435 nm can be assigned to the combination of HOMO − 1 → LUMO and HOMO → LUMO + 1 transitions. Both transitions exhibit the same π → π* character, being HOMO − 1 → LUMO in RHO17 and HOMO → LUMO + 1 in RHO197 (Fig. S12, ESI†). The small peak at around 490 nm can be assigned to the same transitions though with different contributions. In all of the transitions contributing to the spectra the π → π* excitations are localized within one of the two xanthylium cation chromophores. Charge transfer transitions within the dimer are not found to provide a contribution to the spectra.

4 Conclusions

Our calculations allowed us to establish that, in the absence of Pi, the two fluorophores rearrange so as to be stacked, as suggested by some of us a few years ago (Fig. 1).[1] Indeed, in RHO_2–PBP the two RHO fluorophores maintain a stacked dimer conformation. In contrast, in the system with Pi the two fluorophores are largely separated from each other with appreciable conformational freedom concerning their mutual orientation as well as their orientation towards the protein. Whereas RHO17 maintains persistent interactions with PBP in neither RHO_2–PBP·Pi nor RHO_2–PBP, RHO197 interacts with LEU291 in both configurations and strongly with TYR198 in the case of RHO_2–PBP. This suggests that mutations of these residues would lead to considerable structural changes that are expected to be reflected in altered optical spectra. The agreement of simulated CD spectra with experimental ones further corroborates the validity of our structural models. Optical absorption spectra have been simulated with TDDFT methods for the xanthylium chromophores taking the protein environment as well as the conformational flexibility of the systems in aqueous solution at room temperature into account.

Downloaded by Library for Natural Sciences of the RAS on 15/05/2013 11:41:24.
Published on 17 December 2012 on http://pubs.rsc.org | doi:10.1039/C2CP42396K

The absolute values for calculated excitation energies are blue shifted by 0.3–0.4 eV (80–60 nm), which we attribute to well-known deficiencies[53,54] in the accuracy of the DFT/BLYP method. The offset between the spectra of RHO_2–PBP·Pi and RHO_2–PBP as well as the small spacing between the spectral contributions in the case of RHO_2–PBP·Pi are attributed to the different chromopore models adopted for the two systems. The overall shape of the simulated spectra, however, is in fair agreement with that of experimental spectra.

The approach, presented here, also has the possibility of providing an understanding of the detailed mechanism of biosensors signal production, such as the rhodamine–PBP. This can potentially aid design of novel reagentless biosensors, based on the same principle, by allowing detailed predictions of the interaction between fluorophore and protein, or as in this case, two fluorophores on the surface of a protein.

Acknowledgements

MRW was supported by the Medical Research Council, UK (ref. U117512742). MBG gratefully acknowledges the brazilian agency Conselho Nacional de Desenvolvimento Científico e Tecnológico (CNPq) for post-doctoral fellowship (201434/2011-3). Computer time provided by the Jülich Supercomputing Center on JUROPA through the John von Neumann Institute for Computing (NIC – Application number 4789) is gratefully acknowledged.

References

1 M. P. Okoh, J. L. Hunter, J. E. T. Corrie and M. R. Webb, *Biochemistry*, 2006, **45**, 14764–14771.
2 H. Luecke and F. A. Quiocho, *Nature*, 1990, **347**, 402–406.
3 P. S. Ledvina, N. Yao, A. Choudhary and F. A. Quiocho, *Proc. Natl. Acad. Sci. U. S. A.*, 1996, **93**, 6786–6791.
4 M. Brune, J. L. Hunter, S. A. Howell, S. R. Martin, T. L. Hazlett, J. E. T. Corrie and M. R. Webb, *Biochemistry*, 1998, **37**, 10370–10380.
5 M. Brune, J. L. Hunter, J. E. T. Corrie and M. R. Webb, *Biochemistry*, 1994, **33**, 8262–8271.
6 J. E. T. Corrie and J. S. Craik, *J. Chem. Soc., Perkin Trans. 1*, 1994, 2967–2973.
7 M. R. Webb, *Mol. BioSyst.*, 2007, **3**, 249–256.
8 J. E. Selwyn and J. I. Steinfeld, *J. Phys. Chem.*, 1972, **76**, 762–774.
9 R. W. Chambers, T. Kajiwara and D. R. Kearns, *J. Phys. Chem.*, 1974, **78**, 380–387.
10 G. D. Scholes and K. P. Ghiggino, *J. Phys. Chem.*, 1994, **98**, 4580–4590.
11 D. Setiawan, A. Kazaryan, M. A. Martoprawiro and M. Filatov, *Phys. Chem. Chem. Phys.*, 2010, **12**, 11238–11244.
12 K. Ajtai, P. J. K. Ilich, A. Ringler, S. S. Sedarous, D. J. Toft and T. P. Burghardt, *Biochemistry*, 1992, **31**, 12431–12440.
13 P. Ilich, P. Mishra, S. Macura and T. Burghardt, *Spectrochim. Acta, Part A*, 1996, **52**, 1323–1330.
14 M. J. Blackman, J. E. T. Corrie, J. C. Croney, G. Kelly, J. F. Eccleston and D. M. Jameson, *Biochemistry*, 2002, **41**, 12244–12252.
15 B. Z. Packard, D. D. Toptygin, A. Komoriya and L. Brand, *Proc. Natl. Acad. Sci. U. S. A.*, 1996, **93**, 11640–11645.
16 A. Dietrich, V. Buschmann, C. Müller and M. Sauer, *Rev. Mol. Biotechnol.*, 2002, **82**, 211–231.
17 S. Bernacchi and Y. Mély, *Nucleic Acids Res.*, 2001, **29**, e62.
18 B. D. Hamman, A. V. Oleinikov, G. G. Jokhadze, D. E. Bochkariov, R. R. Traut and D. M. Jameson, *J. Biol. Chem.*, 1996, **271**, 7568–7573.
19 R. Car and M. Parrinello, *Phys. Rev. Lett.*, 1985, **55**, 2471–2474.
20 A. Laio, J. VandeVondele and U. Rothlisberger, *J. Chem. Phys.*, 2002, **116**, 6941–6947.
21 E. Runge and E. Gross, *Phys. Rev. Lett.*, 1984, **52**, 997–1000.
22 M. Sulpizi, P. Carloni, J. Hutter and U. Rothlisberger, *Phys. Chem. Chem. Phys.*, 2003, **5**, 4798–4805.
23 M. Sulpizi, U. F. Röhrig, J. Hutter and U. Rothlisberger, *Int. J. Quantum Chem.*, 2005, **101**, 671–682.
24 A. M. Conte, E. Ippoliti, R. Del Sole, P. Carloni and O. Pulci, *J. Chem. Theory Comput.*, 2009, **5**, 1822–1828.
25 A. M. Conte, E. Ippoliti, R. Del Sole, P. Carloni and O. Pulci, *Phys. Status Solidi B*, 2010, **247**, 1920–1924.
26 P. Lupieri, E. Ippoliti, P. Altoè, M. Garavelli, M. Mwalaba and P. Carloni, *J. Chem. Theory Comput.*, 2010, **6**, 3403–3409.
27 N. H. Yao, P. S. Ledvina, A. Choudhary and F. A. Quiocho, *Biochemistry*, 1996, **35**, 2079–2085.
28 Z. Wang, H. Luecke, N. Yao and F. A. Quiocho, *Nat. Struct. Mol. Biol.*, 1997, **4**, 519–522.
29 J. M. Wang, P. Cieplak and P. A. Kollman, *J. Comput. Chem.*, 2000, **21**, 1049–1074.
30 C. I. Bayly, P. Cieplak, W. D. Cornell and P. A. Kollman, *J. Phys. Chem.*, 1993, **97**, 10269–10280.
31 L. Cavallo, M. H. Moore, J. E. T. Corrie and F. Fraternali, *J. Phys. Chem. A*, 2004, **108**, 7744–7751.
32 W. Jorgensen, J. Chandrasekhar, J. D. Madura, R. W. Impey and M. L. Klein, *J. Chem. Phys.*, 1983, **79**, 926–935.
33 U. Essmann, L. Perera, M. L. Berkowitz, T. Darden, H. Lee and L. G. Pedersen, *J. Chem. Phys.*, 1995, **103**, 8577–8593.
34 J. C. Phillips, R. Braun, W. Wang, J. Gumbart, E. Tajkhorshid, E. Villa, C. Chipot, R. D. Skeel, L. Kalé and K. Schulten, *J. Comput. Chem.*, 2005, **26**, 1781–1802.
35 G. J. Martyna, D. J. Tobias and M. L. Klein, *J. Chem. Phys.*, 1994, **101**, 4177–4189.
36 S. Feller, Y. Zhang, R. Pastor and B. Brooks, *J. Chem. Phys.*, 1995, **103**, 4613–4621.
37 X. Daura, K. Gademann, B. Jaun, D. Seebach, W. F. van Gunsteren and A. E. Mark, *Angew. Chem., Int. Ed.*, 1999, **38**, 236–240.
38 A. Becke, *Phys. Rev. A: At., Mol., Opt. Phys.*, 1988, **38**, 3098–3100.
39 C. Lee, W. Yang and R. Parr, *Phys. Rev. B: Condens. Matter Mater. Phys.*, 1988, **37**, 785–789.
40 O. A. von Lilienfeld, I. Tavernelli, U. Rothlisberger and D. Sebastiani, *J. Chem. Phys.*, 2005, **122**, 014113.
41 CPMD, http://www.cpmd.org/, Copyright IBM Corp 1990–2008, Copyright MPI für Festkörperforschung Stuttgart 1997–2001.

 This journal is © the Owner Societies 2013

Downloaded by Library for Natural Sciences of the RAS on 15/05/2013 11:41:24.
Published on 17 December 2012 on http://pubs.rsc.org | doi:10.1039/C2CP42396K

42 W. F. van Gunsteren, S. R. Billeter, A. A. Eising, P. H. P. Hünenberger, P. H. Krüger, A. E. Mark, W. R. P. Scott and I. G. Tironi, *Biomolecular Simulation: The GROMOS96 Manual and User Guide*, Vdf Hochschulverlag AG an der ETH Zürich, Zürich1996.
43 N. Troullier and J. Martins, *Phys. Rev. B: Condens. Matter Mater. Phys.*, 1991, **43**, 1993–2006.
44 O. A. von Lilienfeld, I. Tavernelli, U. Rothlisberger and D. Sebastiani, *Phys. Rev. Lett.*, 2004, **93**, 153004.
45 L. Kleinman and D. M. Bylander, *Phys. Rev. Lett.*, 1982, **48**, 1425–1428.
46 G. Martyna and M. Tuckerman, *J. Chem. Phys.*, 1999, **110**, 2810–2821.
47 M. Dal Peraro, P. Ruggerone, S. Raugei, F. L. Gervasio and P. Carloni, *Curr. Opin. Struct. Biol.*, 2007, **17**, 149–156.
48 B. M. Bulheller, A. Rodger and J. D. Hirst, *Phys. Chem. Chem. Phys.*, 2007, **9**, 2020–2035.
49 B. M. Bulheller and J. D. Hirst, *Bioinformatics*, 2009, **25**, 539–540.
50 N. A. Besley and J. D. Hirst, *J. Am. Chem. Soc.*, 1999, **121**, 9636–9644.
51 M. T. Oakley and J. D. Hirst, *J. Am. Chem. Soc.*, 2006, **128**, 12414–12415.
52 D. M. Rogers and J. D. Hirst, *J. Phys. Chem. A*, 2003, **107**, 11191–11200.
53 D. Jacquemin, V. Wathelet, E. A. Perpète and C. Adamo, *J. Chem. Theory Comput.*, 2009, **5**, 2420–2435.
54 D. Jacquemin, B. Mennucci and C. Adamo, *Phys. Chem. Chem. Phys.*, 2011, **13**, 16987–16998.
55 A. Pedone and V. Barone, *Phys. Chem. Chem. Phys.*, 2010, **12**, 2722–2729.
56 A. Pedone, J. Bloino, S. Monti, G. Prampolini and V. Barone, *Phys. Chem. Chem. Phys.*, 2010, **12**, 1000–1006.
57 V. Barone, J. Bloino, S. Monti, A. Pedone and G. Prampolini, *Phys. Chem. Chem. Phys.*, 2010, **12**, 10550–10561.
58 A. D. Simone, J. E. T. Corrie, R. E. Dale, M. Irving and F. Fraternali, *J. Am. Chem. Soc.*, 2008, **130**, 17120–17128.
59 There is a H-bond between the nitrogen in the tail of the benzoate side group of the RHO closest to the protein surface (RHO197) and the backbone carbonyl oxygen of the LEU291. This H-bond is, however, rather weak as it is observed in the entire trajectory for only ~7% of the time.